This article has been accepted for publication in IEEE Transactions on Sustainable Energy. This is the author's version which has not been fully edited and content may change prior to final publication. Citation information: DOI 10.1109/TSTE.2022.3188250

Probabilistic Rolling-Optimization Control for Coordinating the Operation of Electric Springs in Microgrids with Renewable Distributed Generation

Darwin A. Quijano, Antonio Padilha-Feltrin, *Senior Member, IEEE* and João P. S. Catalão, *Fellow, IEEE.*

***Abstract*—Electric spring (ES) is a novel smart grid technology developed to facilitate the integration of renewable generation by controlling the demand of non-critical loads (NCLs). The utilization of ES to provide a single service such as voltage or frequency regulation, validated in a setup consisting of a single ES, has been extensively investigated. However, to take full advantage of this technology, it is necessary to develop control strategies to coordinate the operation of multiple distributed ESs to provide multiple services in power systems. To this end, this paper presents a rolling-optimization control strategy to coordinate the operation of multiple ESs for voltage regulation, congestion management and cost minimization of the real-time deviations from the scheduled energy exchanges with the grid in microgrids with renewable generation. The strategy is for centralized implementation, and includes a probabilistic optimal power flow-based optimization engine that finds the voltage references of ESs for each control interval taking into account generation variability and uncertainties. NCLs consist of electric water heaters, which are modeled taking into account physical constraints and the hot water demand. Simulations were carried out in two test systems with 14 and 33 buses.**

***Index Terms*—Electric spring, electric water heater, microgrid, renewable energy, rolling-optimization.**

NOMECLATURE

i, ij, t, n	Indices for bus, line segment, time interval and scenario;
$E_{i,t,n}$	Thermal energy stored in the EWH;
$E^l_{i,t,n}, E^u_{i,t,n}$	Thermal energy stored in the lower and upper water layers of the EWH's tank;
$L_i, L^l_{i,t,n}, L^u_{i,t,n}$	Total EWH's tank volume, volume of lower layer, and volume of upper layer;
T^l, T^u, T^a	Cold water temperature, hot water temperature and ambient temperature;
c, m	Specific heat capacity and density of water;
$P^a_{i,t,n}$	Total EWH heat loss;
$P^{al}_{i,t,n}, P^{au}_{i,t,n}$	Heat loss from the lower and upper water layers in the EWH's tank;
$P^{lu}_{i,t,n}$	Thermal conduction between the lower and upper water layers in the EWH;
P^{alu}_i	Maximum EWH heat loss;
$W_{i,t}$	Rate of hot water draw from the EWH;
η	Efficiency of the lower heating element;
Δ^c	Duration of the control interval;
Δ^d	Lead time for set points calculation;
T_p	Duration of planning horizon;
$P^{NCL}_{i,t,n}$	Power of the lower heating element;
$E^a_i, E^{max}_i, E^{min}_i$	Thermal energy stored in the EWH when it is full of water at ambient temperature, hot water, and cold water;
$SOTC_{i,t,n}$	State of thermal charge of the EWH;
τ	Heat loss time constant;
$V^{NCL}_{i,t,n}$	Voltage supplied to the NCL;
$V^{ES}_{i,t,n}$	Output voltage of the ES;
$V_{i,t,n}$	Voltage at bus i;
R^{NCL}_i	Resistance of the lower heating element;
$Q^{ES}_{i,t,n}$	Reactive power injected by the ES;
$P^{CL}_{i,t,n}, Q^{CL}_{i,t,n}$	Active and reactive CL power;
$P^Z_{i,t}, P^I_{i,t}, P^P_{i,t}$	Share of the constant impedance, constant current, and constant power components in the total CL active power;
$Q^Z_{i,t}, Q^I_{i,t}, Q^P_{i,t}$	Share of the constant impedance, constant current, and constant power components in the total CL reactive power;
$P^{av}_{i,t,n}$	Available active power from the DG;
$\omega_{t,n}$	Generation level relative to nominal capacity;
P^{ic}_i	DG Installed capacity;
$P^g_{i,t,n}, Q^g_{i,t,n}$	Active and reactive powers injected by the DG;
$P^{curt}_{i,t}$	Generation curtailment from the DG;
$\theta_{i,t}$	DG Power factor angle;
θ^-, θ^+	DG Minimum and maximum power factor angles
$P_{ij,t,n}, Q_{ij,t,n}$	Active and reactive power flows in the line segments;
$p_{i,t,n}, q_{i,t,n}$	Net active and reactive powers injected at bus i;
r_{ij}, x_{ij}	Resistance and reactance in the line segments;
$I^{sqrt}_{ij,t,n}$	Magnitude squared of the current in the line segments;
V^n	Nominal voltage;
$P^s_{i,t}$	Scheduled active power exchange with the main grid;
$P^{up}_{i,t,n}, P^{dn}_{i,t,n}$	Upward and downward deviations from the scheduled active power exchanges;
$Q^s_{i,t,n}$	Reactive power exchange with the main grid;
V^{min}, V^{max}	Minimum and maximum voltage limits;
$\bar{I}_{ij}$	Maximum current flow in the line segment;
ρ_n	Probability of scenario n;
C^s_t	Day-ahead energy prices.
$\kappa^{up}_t, \kappa^{dn}_t$	Upward and downward imbalance prices.

This work was supported by São Paulo Research Foundation (FAPESP) under grants: 2018/06451-8, 2020/12401-3 and 2015/21972-6, by CNPq under grant: 310299/2020-9, and by CAPES (code finance 001).

D.A. Quijano is with Universidade Estadual Paulista–UNESP, Ilha Solteira 15385-000, Brazil, and INESC TEC, 4200-465, Porto, Portugal (e-mail: alexisqr@yahoo.es).

A. Padilha-Feltrin is with Universidade Estadual Paulista–UNESP, Ilha Solteira 15385-000, Brazil (e-mail: padilha@dee.feis.unesp.br).

J.P.S Catalão is with the Faculty of Engineering of the University of Porto, 4200-465 Porto, Portugal, and INESC TEC, 4200-465 Porto, Portugal (e-mail: catalao@fe.up.pt)

I. INTRODUCTION

The development of microgrids is driven by the potential benefits of locally supplying the electricity demand using

distributed energy resources (DERs) such as distributed generation (DG). Some of these benefits include improving sustainability in energy generation, reducing congestion and energy losses in transmission systems, and enhancing reliability and quality of power supply to end users. Large penetration levels of renewable energy resources (RES)-based DG in microgrids are expected to provide the benefits of local generation; however, their integration into the system presents several challenges.

The main drawbacks of interconnecting RES-based DG in microgrids are related to the variability and uncertainty of power production, which can affect voltage regulation, congestion levels and balance of supply and demand [1]. The common approaches to address these drawbacks include the use of battery energy storage systems (BESSs) and regulation reserves based on dispatchable generation [2], [3]. Demand side management has also been demonstrated to be effective for RES-based DG integration [4], [5]. In this respect, water heater loads have a significant potential to participate in demand side management. The demand of hot water represents 14% of the total residential energy consumption in the European Union and 18% in the USA [6]. However, until recently, the effectiveness of managing water heater loads for RES-based DG integration was undermined by the discrete on/off nature of the thermal control loops that drive electric water heaters (EWHs) [7]. This limitation can be now overcome by interfacing EWHs with electric springs (ESs) and turning them into smart loads.

ES is a novel smart grid technology developed to improve the controllability of non-critical loads (NCL) for demand side management. An ES consists in a power electronic device that is installed in series with impedance-type NCLs such as EWHs, air conditioners and refrigerators [8], [9]. By generating a controllable voltage, the ES can regulate the voltage and power demand of the NCL while injecting reactive power into the system [8]. Generally, loads can be classified into critical loads (CLs) and NLCs depending on their tolerance to voltage fluctuations. The first applications of ESs were developed to damp electric oscillations and provide CLs with a tightly regulated voltage in systems with high penetration of RES-based DG [8], [10]. Later, the use of ESs was expanded to mitigate frequency fluctuations [11]. In these initial studies, the performance of ESs was evaluated considering a single locally-controlled unit. However, the system-level impact of ESs will only be released if multiple units are distributed across the distribution systems and the associated control strategies are developed. To address this problem, Akhtar *et al.* [12] proposed a droop control method to operate multiple ESs for frequency regulation. In [13], the coordination of multiple ESs for bus voltage regulation was achieved through a consensus algorithm.

With the increasing interest in the ES technology, several other applications have been proposed in the literature. For example, in [9], ESs are used to regulate bus voltage and power and provide power factor correction in distribution systems. In [14], an integrated configuration consisting of an ES connected with a photovoltaic system is applied to achieve dynamic supply-demand balance in distribution systems. In [15], the utilization of ESs to provide constant power to loads with varying impedance is investigated. The studies in [9], [14], [15] demonstrated the proposed ES applications considering a single locally-controlled ES. In [16], a strategy based on a centralized predictive control is proposed to manage the operation of multiple ESs to mitigate power losses in an islanded microgrid. The authors of [17] developed an optimization model for the operation of a transactive energy system that consists of multiple microgrids with ESs used to minimize the total bus voltage deviations. The problem of allocating ESs to provide bus voltage regulation in distribution systems is addressed in [18] through an optimization-based approach.

Most of the existing works that deal with the problem of coordinating multiple ESs [12], [13], [16]–[20] are focused on a single application, for example, bus voltage regulation. However, a practical implementation of ESs will require them to simultaneously provide multiple services in a coordinated manner. To this end, this work proposes a rolling-optimization control strategy that coordinates the operation of multiple ESs to simultaneously provide voltage regulation, congestion management and cost minimization of the real-time deviations from the scheduled energy exchanges with the grid in microgrids with high penetration levels of RES-based DG. The strategy is designed for centralized implementation and is based on a probabilistic optimal power flow formulation that takes into account uncertainties of RES-based DG power production. To the best of the author's knowledge, ESs have not been used to simultaneously provide these services and probabilistic approaches have not been proposed to take into account uncertainties of RES-based DG power production when coordinating the operation of ESs.

In addition, while the consumption of NCLs connected with ESs is flexible, users satisfaction still needs to be ensured when NCLs participate in demand side management. To achieve this, NCLs must be modeled taking into account both their electrical and physical constraints. In the literature, only a few works have included detailed NCL models. In [19], a realistic EWH model is considered within a distributed control scheme designed to coordinate multiple ESs for overvoltage prevention. Zhang *et al.* [20] propose a scheduling strategy to control the power demand of air conditioners connected with ESs to smooth the peak-valley difference in the distribution system. In [21], an ice-thermal storage system installed with an ES is operated to provide voltage regulation and dynamic supply-demand balance in a distribution system. In [22], a model predictive control strategy is designed to minimize the operational cost of a microgrid through the operation of a water heater system connected with an ES. Although these works include realistic models of NCLs, they either consider a single ES [21], [22] or consider multiple ESs operated for a single application [19], [20].

In this work, NCLs are represented by EWHs, which are modeled considering their electrical and physical constraints as well as the hot water consumption profile of the users. This configuration of EWH with ES works as a thermal storage system that stores energy at times of generation surplus for later use at times of generation deficit. When deployed in

microgrids, ESs are expected to reduce the dependence on large-scale BESSs, which have high investment cost, limited capacity and environmental impact. The ability of ESs to reduce BESSs requirements for voltage regulation in distribution systems was demonstrated in [10], [19]. Because of this, this work does not consider the presence of BESSs in the microgrid.

The major contributions of this paper are listed as follows:

- A rolling-optimization control strategy with multi-minute control interval for coordinating the operation of multiple ESs to provide voltage regulation, congestion management and cost minimization of the real-time deviations from the scheduled energy exchanges with the grid in microgrids with high penetration of RES-based DG.
- A probabilistic optimal power flow-based optimization engine for centralized implementation that finds the ES voltage references for each control interval based on predictions of demand and generation, and taking into account the uncertain behavior of RES-based DG power production. A probabilistic formulation is proposed so that optimal decisions are made taking into account the possible realizations of RES-based DG power production within each control interval, avoiding bus voltage and line thermal limits violations. To the best of the author's knowledge, this is the first time uncertainties are considered in the problem of coordinating the operation of ESs.

Table I shows a comparison of the proposed control strategy for ESs with those found in the literature.

The remainder of this paper is organized as follows. Section II describes the microgrid control architecture and the rolling-optimization control strategy. Section III presents the model of the optimization engine. The characterization of the wind power uncertainties and the scenarios generation process are described in section IV. The computational implementation is discussed in section V. Case studies and discussions are provided in section VI. Finally the conclusions are presented.

II. Microgrid control architecture and rolling-optimization control strategy

In a microgrid, DERs and controllable loads are managed by the microgrid control system, which is responsible of ensuring the continuous power supply to loads with acceptable voltage and frequency characteristics. The microgrid control system integrates local and supervisory controllers and can be physically implemented in a variety of ways, including distributed and centralized [23]. The proposed rolling-optimization control strategy is designed to be implemented through a centralized microgrid control system, which is composed of a microgrid central controller (MGCC), local controllers of DERs and loads, and a communication system to exchange information between the MGCC and the local controllers. A microgrid operating in grid-connected mode, with DERs consisting of wind-based DG with controllable power factor and curtailable active power generation, is considered. Other types of RES-based DG can be easily integrated into the model and similar performance analyzes can be carried out considering the different generation profiles. Loads supplied by the microgrid are classified into CLs and NCLs. Here, NCLs installed with ESs consist of EWHs for residential hot water consumption.

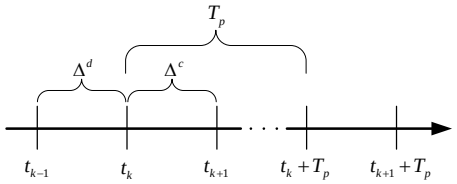

Fig. 1. Scheme of the rolling-optimization strategy.

In the proposed strategy, optimal set points (i.e., ES voltage references, DG active power curtailment, and DG power factor) are determined at the MGCC to minimize the cost of the real-time energy deviations and avoid bus voltage and line thermal limits violations. A scheme of the process carried out by the rolling-optimization control strategy is shown in Fig. 1. At time $t_k - \Delta^d$, the optimization engine optimizes the system operation for the finite window $[t_k,\ t_k + T_p]$ based on predictions of wind power generation, CL demand and hot water demand, and taking into account uncertainties of wind power generation. These predictions are obtained from measured values of previous control intervals, which are sent to the MGCC by the local controllers. Uncertainties are taken into account through a scenario-based approach that simulates the possible realization wind power generation within each control interval. In practice, the leadtime Δ^d accounts for the processing time and communication delay, and in this work is assumed to be equal to the duration of the control interval Δ^c. From the obtained optimal set points, those corresponding to the control interval $[t_k,\ t_{k+1}]$ are sent to the local controllers for implementation, whereas the remaining are disregarded. After that, the prediction horizon is rolled forward and the process is repeated with new predicted data at t_k.

The proposed strategy determines the optimal set points for the current control interval taking into account the future system behavior, which is subject to the changing conditions of generation and demand. These set points are to be held throughout the length of the multi-minute control interval, which is adopted to avoid solving the optimization problem too frequently. A probabilistic formulation of the optimization problem allows to take into account the possible realizations of wind power generation within the control intervals and therefore seeks to maintain the voltage and power flow levels within limits. Uncertainties of CL demand and hot water demand are not considered because the predicted values are not expected to have significant variations within control intervals.

III. Optimization engine

This section describes the model used to optimize the microgrid operation for the prediction horizon. The control variables represent the set points of controllable resources, which include DG power factor, DG curtailment and ESs voltage output. To incorporate the variability and uncertainty of wind power into the model, a probabilistic approach, in which scenarios of wind power with their respective probability of occurrence are sampled from a Beta probability density

TABLE I
LITERATURE REVIEW OF RELATED WORKS

Ref.	year	Multiple ES	NCL physical constraints	Uncertainties	ES application
[8]	2012				Bus voltage regulation
[10]	2013				Bus voltage regulation
[11]	2015				Bus voltage and frequency regulation
[12]	2015	✓			Frequency regulation
[13]	2017	✓			Bus voltage regulation
[9]	2017				Bus voltage and power regulation, and power factor correction
[14]	2019				Dynamic supply-demand balance
[15]	2019				Provide constant power to a load with varying impedance
[16]	2020	✓			Bus voltage regulation and mitigation of power losses
[17]	2020	✓			Bus voltage regulation in a transactive energy system
[18]	2021	✓			Allocation of ESs for bus voltage regulation
[19]	2020	✓	✓		Bus voltage regulation
[20]	2021	✓	✓		Smooth peak-valley difference
[21]	2017		✓		Bus voltage regulation and dynamic supply-demand balance
[22]	2019		✓		Minimize operational cost
Proposed	–	✓	✓	✓	Bus voltage regulation, congestion management, and Cost minimization of real-time energy deviations

function (PDF) [24], [25], is proposed. This approach assigns to each control interval a number of values of wind power generation that the optimal set points must satisfy.

A. Objective function

This work proposes to coordinate the operation of ESs to minimize the cost of the real-time deviations from the day-ahead scheduled energy exchanges with the main grid (payments made for upward deviations minus payments received for downward deviations) while managing bus voltage levels and line congestion. This formulation is applicable to microgrids that trade the energy exchanges with the main grid in a day-ahead market and are financially accountable for the real-time energy deviations [26], [27]. The objective function is formulated as follows:

$$\min \sum_{t\in\Omega_t}\sum_{n\in S}\rho_n\Delta^c(\kappa_t^{up}P_{e,t,n}^{up}-\kappa_t^{dn}P_{e,t,n}^{dn}), \qquad (1)$$

where e denotes the bus at which the point of common coupling with the main grid is located. The scheduled energy exchange with the main grid at a given time interval can be energy import or export depending on the value of the predicted net load (demand minus generation) in the microgrid. Upward deviations from the scheduled energy exchanges ($\Delta^c P_{e,t,n}^{up}$) occur when the real-time net load is greater than the scheduled value (energy shortage). Similarly, downward deviations ($\Delta^c P_{e,t,n}^{dn}$) occur when the real-time net load is lower than the scheduled value (energy surplus). Here, the energy shortage is charged with an imbalance price κ^{up}, and the energy surplus is paid for with an imbalance price κ^{dn} [27]. Thus, (1) minimizes the payments that the microgrid makes for the downward deviations and maximizes the payments that the microgrid receives for the upward deviations. The objective function (1) is subject to a set of constraints defined in the following subsections.

B. Model of electric water heater

A realistic model of an EWH must take into account its electrical and thermal characteristics, as well as the hot water demand. Fig. 2 shows the configuration of the EWH composed of a tank, two heating elements and their respective thermostats. The water in the tank is vertically divided into three layers: a lower layer with cold water at temperature T^l, an upper layer with hot water at temperature T^u, and a mixing layer in between [7]. The cold water that enters the tank to replace the consumed hot water remains in a layer at the bottom of the tank because is denser than hot water. The mixing layer moves up and down depending on the content of hot water in the tank. This layer behaves as a dynamic natural barrier that maintains the hot water layer separated from the cold one [28]. In this model, the thickness of the mixing layer is assumed to be zero [7], [19]. In practice, the upper heating element is turned on only when the cold-water layer reaches a critical level and is therefore disregarded [19]. The total thermal energy stored in the EWH is determined by the volumes of cold water at temperature T^l and hot water at temperature T^u as follows:

$$E_{i,t,n}=E_{i,t,n}^l+E_{i,t,n}^u=cmL_{i,t,n}^lT^l+cmL_{i,t,n}^uT^u. \qquad (2)$$

The change in the stored thermal energy between two consecutive time intervals is described by the dynamic thermal energy balance equation expressed as follows:

$$E_{i,t,n}^l=E_{i,t-1,n}^l+\Delta^c\left[cmW_{i,t}T^l+\eta P_{i,t,n}^{NCL}-P_{i,t,n}^{al}+P_{i,t,n}^{lu}\right], \qquad (3)$$

$$E_{i,t,n}^u=E_{i,t-1,n}^u-\Delta^c\left[cmW_{i,t}T^u+P_{i,t,n}^{au}+P_{i,t,n}^{lu}\right], \qquad (4)$$

$$E_{i,t,n}=E_{i,t,n}^l+E_{i,t,n}^u=E_{i,t-1,n}+\Delta^c\left[\eta P_{i,t,n}^{NCL}+cmW_{i,t}(T^l-T^u)-P_{i,t,n}^a\right]. \qquad (5)$$

The heat loss from the water in the EWH to the ambient air is calculated according to the following expression [19]:

$$P_{i,t,n}^a=P_{i,t,n}^{al}+P_{i,t,n}^{au}=P_i^{alu}\frac{E_{i,t,n}-E_i^a}{E_i^{\max}-E_i^a}, \qquad (6)$$

where, $E_i^a=cmL_iT^a$, $E^{max}=cmL_iT^u$ and $L_i=L_{i,t,n}^l+L_{i,t,n}^u$. P_i^{alu} is obtained from

$$P_i^{alu}=cmL_i(T^u-T^a)/\tau, \qquad (7)$$

where, τ is a constant that indicates the time it takes the thermal losses to bring down the water temperature from T^u

This article has been accepted for publication in IEEE Transactions on Sustainable Energy. This is the author's version which has not been fully edited and content may change prior to final publication. Citation information: DOI 10.1109/TSTE.2022.3188250

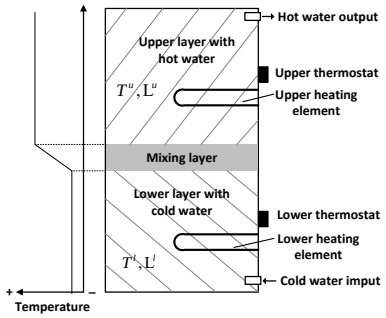

Fig. 2. Configuration and temperature profile of an EWH [7].

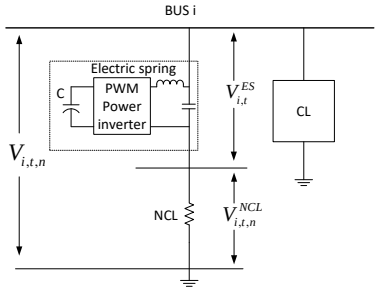

Fig. 3. Diagram of connection of electric spring.

to T^a, and in this work is set to 120 h [7]. The measure used to indicate the amount of thermal energy stored in the EWH is the state of thermal charge (SOTC) defined as follows:

$$SOTC_{i,t,n} = \frac{E_{i,t,n} - E_i^{\min}}{E_i^{\max} - E_i^{\min}}, \tag{8}$$

where $E_i^{\min} = cmL_iT^l$. The SOTC is limited to minimum and maximum values as follows:

$$SOTC^{min} \leq SOTC_{i,t,n} \leq SOTC^{max}. \tag{9}$$

The conventional approach used to control the power demand of the EWH [denoted by $P_{i,t,n}^{NCL}$ in (5)] uses an on/off thermal control loop determined by the thermostat. Under this control, $P_{i,t,n}^{NCL}$ is equal to the rated power when the lower heating element is switched on and equal to zero when the lower heating element is switched off [7]. In this work, the lower heating element is connected in series with an ES to have a continuous regulation of $P_{i,t,n}^{NCL}$. From (5) it can be seen that the time dependent data required from the EWHs to control the ESs are the predictions of hot water demand $W_{i,t}$ that are obtained from measured values of previous control intervals.

C. Electric spring operation and capability

Fig. 3 shows the configuration of an ES connected in series with a NCL (in this case a pure resistive NCL). The combination of an ES with a NCL is commonly known as smart load [11], [13]. In parallel with the smart load, the CL is connected directly to the microgrid bus. This work considers the first generation of ES, which consists of an inverter with a capacitor installed on the dc link side and an inductor-capacitor (LC) filter on the ac side [8]. This type of ES can only inject reactive power because it does not involve battery storage. To ensure that the ES only injects reactive power, its output voltage must be maintained perpendicular to the current vector of the NCL [22]. The relationship between the magnitudes of voltages in Fig. 3 is expressed as

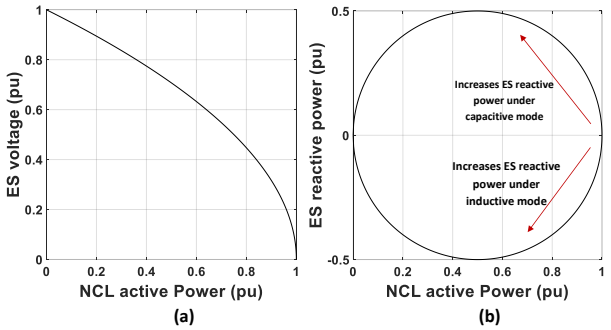

Fig. 4. Change of NCL active power for (a) change is ES voltage and (b) change in ES reactive power.

$$V_{i,t,n}^{NCL} = \sqrt{V_{i,t,n}^2 - V_{i,t}^{ES^2}}. \tag{10}$$

The NCL active power demand is a function of the supply voltage $V_{i,t,n}^{NCL}$ and is expressed as

$$P_{i,t,n}^{NCL} = \left(V_{i,t,n}^{NCL^2}\right)/R_i^{NCL}, \tag{11}$$

The reactive power injected by the ES is a function of $V_{i,t}^{ES}$ and the NCL current, and can be expressed as

$$Q_{i,t,n}^{ES} = \left(V_{i,t}^{ES} V_{i,t,n}^{NCL}\right)/R_i^{NCL}. \tag{12}$$

In this work, as in [22], it is assumed that $V_{i,t}^{ES}$ takes positive values for inductive operation and negative values for capacitive operation of the ES. From (10), to ensure that $V_{i,t,n}^{NCL}$ only takes positive and real values, $V_{i,t}^{ES}$ is limited by

$$-V_{i,t,n} \leq V_{i,t}^{ES} \leq V_{i,t,n}. \tag{13}$$

It is worth noting that $V_{i,t}^{ES}$ must hold for all values of wind power within the control interval and is therefore not indexed by n. Through the dynamic control of the ES voltage $V_{i,t}^{ES}$ it is possible to regulate the power delivered to the NCL. For example, the ES voltage can be increased to reduce the NCL consumption when there is energy deficit in the microgrid.

The operating range of a smart load composed of an ES and a pure resistive NCL rated at 1 pu ($R_i^{NCL} = 1$ pu) is shown in Fig 4. To draw this figure, the values of $V_{i,t,n}^{NCL}$, for $V_{i,t}^{ES}$ ranging from 0 to 1 pu, and with $V_{i,t,n}$ assumed to be 1 pu, are calculated using (10). Then, $P_{i,t,n}^{NCL}$ and $Q_{i,t,n}^{ES}$ are calculated using (11) and (12), respectively. Fig 4(a) shows that, for a pure resistive NCL, increasing the ES voltage $V_{i,t}^{ES}$ always leads to a reduction in the NCL active power $P_{i,t,n}^{NCL}$ with respect to the rated value. This is because, according to (11), the NCL active power depends directly on the NCL voltage, which decreases when the ES voltage is increased according to (10). Fig. 4(b) describes the smart load capability curve in which the smart load operating range is limited to the perimeter of the circumference. It is observed that reducing the NCL active power requires the injection of reactive power by the ES, which can be either inductive or capacitive. When reducing the NCL active power, the reactive power injected by the ES increases up to a maximum value that is reached when the NCL power is equal to 0.5 p.u. after which it begins to decrease.

D. Critical loads model

CLs require a supply voltage regulated within a strict range to function properly. Like with NCLs, the power demand of a variety of CLs is dependent on the magnitude of the supply

voltage [26]. To account for this dependency, CLs are modeled using the ZIP load model as follows:

$$P^{CL}_{i,t,n} = P^{Z}_{i,t} V^{2}_{i,t,n} + P^{I}_{i,t} V_{i,t,n} + P^{P}_{i,t}, \quad (14)$$

$$Q^{CL}_{i,t,n} = Q^{Z}_{i,t} V^{2}_{i,t,n} + Q^{I}_{i,t} V_{i,t,n} + Q^{P}_{i,t}. \quad (15)$$

In this model, CLs are represented by a combination of constant impedance (Z), constant current (I) and constant power (P) components. The share of each component in the total CL active (reactive) power demand is given by the parameters $P^{Z}_{i,t}$, $P^{I}_{i,t}$ and $P^{P}_{i,t}$ ($Q^{Z}_{i,t}$, $Q^{I}_{i,t}$ and $Q^{P}_{i,t}$).

E. Distributed generation model

In this work, wind-based DG with controllable power factor and curtailable active power is considered. The active power available to be injected by a DG unit is given by:

$$P^{av}_{i,t,n} = \omega_{t,n} P^{ic}_{i}, \quad (16)$$

where $\omega_{t,n}$ is a random parameter whose values are sampled for each time interval t and scenario n from a Beta PDF as will be shown later. Depending on the DG installed capacity P^{ic}_{i} and the generation level $\omega_{t,n}$, injecting the available active power can lead to microgrid constraints violations. Curtailment of the DG available active power is an option to alleviate such problems [26], [29]. The following formulation is used for generation curtailment:

$$P^{g}_{i,t,n} = P^{av}_{i,t,n} - P^{curt}_{i,t}, \quad (17)$$

$$P^{curt}_{i,t} \leq P^{av}_{i,t,n}, \quad (18)$$

where, $P^{curt}_{i,t}$ is defined as a control variable within the model. For each control interval, the optimization will find a value of $P^{curt}_{i,t}$ for all scenarios of wind power generation. In general, limiting the DG power production is an expensive solution and its application will be limited to situations when other solutions are exhausted. Although it is not explicitly represented in the objective function (1), the adopted formulation minimizes the generation curtailment due to its direct relationship with the downward and upward deviations from the scheduled energy exchanges. In other words, by harnessing all the energy from the generators, it is avoided to increase the energy shortage and/or reduce the energy surplus in the microgrid, which is necessary to minimize the imbalance cost. In addition, the reactive power provided by the DG is limited to a range of power factors as follows:

$$\theta^{-} \leq \theta_{i,t} \leq \theta^{+}, \quad (19)$$

where, $\theta_{i,t}$ is a control variable with a single value determined for each control interval.

F. Power flow equations

The complex power flows at each node of the microgrid are described by the DistFlow equations simplified according to the assumptions made in [32].

$$\sum_{ij \in \Omega_l} P_{ij,t,n} = P_{hi,t,n} - r_{hi} I^{sqr}_{hi,t,n} + p_{i,t,n}, \quad (20)$$

$$\sum_{ij \in \Omega_l} Q_{ij,t,n} = Q_{hi,t,n} - x_{hi} I^{sqr}_{hi,t,n} + q_{i,t,n}, \quad (21)$$

$$V_{j,t,n} = V_{i,t,n} - \left(r_{ij} P_{ij,t,n} + x_{ij} Q_{ij,t,n}\right) / V^{n2}, \quad (22)$$

$$I^{sqr}_{hi,t,n} = \left(P^{2}_{hi,t,n} + Q^{2}_{hi,t,n}\right) / V^{n2}. \quad (23)$$

where, i is the reference node, h is the node upstream node i, $j|ij \in \Omega_l$ is the set of nodes downstream node i, and Ω_l is the set of nodes in the microgrid. $p_{i,t,n}$ and $q_{i,t,n}$ are the net active and reactive power injections at node i defined as follows:

$$p_{i,t,n} = P^{g}_{i,t,n} - P^{CL}_{i,t,n} - P^{NCL}_{i,t,n} + (P^{s}_{i,t} + P^{up}_{i,t,n} - P^{dn}_{i,t,n}), \quad (24)$$

$$q_{i,t,n} = Q^{g}_{i,t,n} - Q^{CL}_{i,t,n} + Q^{ES}_{i,t,n} + Q^{s}_{i,t,n}. \quad (25)$$

The terms that compose $p_{i,t,n}$ and $q_{i,t,n}$ are nonzero only at those buses where the elements they represent exist. For example, $P^{g}_{i,t,n}$ is different from zero only at buses with DG. The terms in parentheses in (24) define the active power exchange with the main grid, which is represented as the sum of the scheduled value and the upward and downward adjustments. To ensure the adequate operation of CLs, the voltage variations at each node are limited to a range defined in (26). The current flow at each line segment is limited to a maximum value as shown in (27).

$$V^{min} \leq V_{i,t,n} \leq V^{max}, \quad (26)$$

$$0 \leq I^{sqr}_{ij,t,n} \leq \bar{I}^{2}_{ij}. \quad (27)$$

IV. Generation of scenarios of wind power

The proposed rolling-optimization control strategy determines the optimal set points for each control interval based on predicted profiles of demand and generation with multi-minute resolution. To cater for uncertainties and fluctuations of wind power within each control interval, the optimization is performed over a set of scenarios that describe the possible realizations of wind power. This approach assumes that the realizations of wind power follows a Beta PDF from which the set of scenarios is sampled. The adequacy of the Beta PDF to model the wind power was demonstrated in [24] and [25] by comparing it with the distribution of real data. In addition, the Beta PDF is easy to handle since it only depends on two parameters α and β, and its values are limited to the interval [0,1] as it happens with the normalized wind power. The Beta PDF is defined as follows:

$$f_{\bar{\omega}_t}(\omega_t) = \frac{{\omega_t}^{\alpha_t - 1} \cdot (1 - \omega_t)^{\beta_t - 1}}{B(\alpha_t, \beta_t)}, \quad (28)$$

$$B(\alpha_t, \beta_t) = \int_0^1 {\omega_t}^{\alpha_t - 1} \cdot (1 - \omega_t)^{\beta_t - 1} d\omega_t, \quad (29)$$

where, $0 \leq \omega_t \leq 1$ and $\alpha_t, \beta_t > 0$. Equation (28) models for each time interval t the occurrence of wind power values ω_t when a certain value $\bar{\omega}_t$ has been predicted. The parameters α_t and β_t are functions of the predicted mean value $\bar{\omega}_t$ and the standard deviation σ_t as follows:

$$\alpha_t = \frac{(1 - \bar{\omega}_t) \cdot \bar{\omega}_t^{2}}{\sigma^{2}} - \bar{\omega}_t, \quad (30)$$

$$\beta_t = \frac{1 - \bar{\omega}_t}{\bar{\omega}_t} \cdot \alpha_t. \quad (31)$$

The relationship between $\bar{\omega}_t$ and σ_t is given by $\sigma_t = 0.5 \cdot \bar{\omega}_t \cdot (1 - \bar{\omega}_t)$ [24].

The process of generating scenarios of wind power consists of two steps. In the first step, a large set of scenarios $\bar{S}$ with

equal probability of occurrence is randomly generated from the PDF (28). Here, a scenario consists of a profile of wind power for the current prediction horizon under evaluation. The second step uses the simultaneous backward reduction technique (SBR) described in [33] to reduce the set $\bar{S}$ to a set S that efficiently approximates the continuous PDF (28). The SBR method determines a reduced scenario set $\bar{S}$ by removing a scenario subset J from the original scenario set S. This is a heuristic method that iteratively determines the scenarios to be removed based on a scenario distance metric. Each scenario in the reduced set is assigned with a probability of occurrence ρ_n. Numerical results reported in [33] demonstrate that this method performs well in terms of solution time and accuracy to produce a reduced scenario set. In addition, the performance of the SBR method applied to a power systems application of stochastic programming was demonstrated in [34].

V. Implementation

The optimization problem that is successively solved to determine the optimal set points of the controllable resources for each control interval is defined by the objective function (1) subject to constraints (5)–(27). This problem is nonlinear with continuous variables. The source of nonlinearities are the ES constraints (10)–(12), the constraints corresponding to the CL power (14) and (15), and the constraint that defines the magnitude squared of the line current (23). The rolling-optimization algorithm was coded in the algebraic modeling language AMPL and the commercial solver KNITRO was used for the optimization steps. The KNITRO solver is let to automatically choose the solution algorithm and it uses the interior-point/barrier direct method.

VI. Simulations and Results

Results were obtained from a real microgrid in Guangdong province, China, and the IEEE 33-bus system, which have been adapted for the simulations performed here. Tests are performed for a period of 24 hours with a control interval of 10 min Δ^c = 10 min) and a prediction horizon of 4 hours (T_p = 4 hours). The average time required to solve the proposed optimization problem for each control interval is 1.4 and 1.8 minutes for the Guangdong and the IEEE 33-bus systems, respectively, using a computer with a processor Intel Core i7-6700HQ and 8 GB of RAM. It is observed that this processing time is lower than the leadtime Δ^d of 10 minutes adopted in this work for real-time implementation.

A. Guangdong system

The diagram together with the line data and the CL peak values of this microgrid are shown in Fig. 5 [35]. CLs are assumed to have a power factor of 0.9 lagging, and are composed of a mix of 30% constant impedance, 50% constant current and 20% constant power components. The total CL in the microgrid is 7.8 MW. Wind farms are installed at buses 9, 10, 13 and 14, and they are limited to operate between a 0.9 lagging to 0.9 leading power factor range. Smart loads composed of EWHs and ESs are located at buses 1, 7, 8 and 12. All EWHs have identical capacities and a peak hot water demand of 500 kW, calculated assuming an inlet water

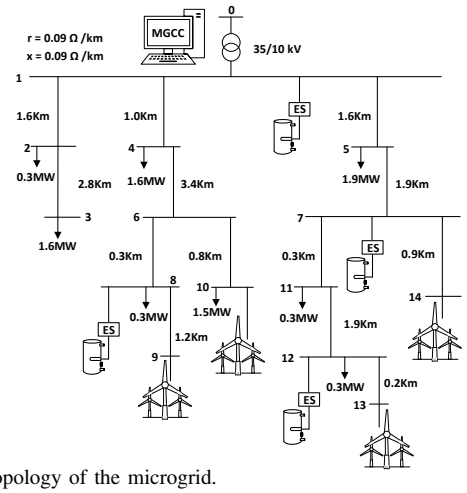

Fig. 5. Topology of the microgrid.

temperature of 20 °C (T^l = 20 °C), a set temperature of 65 °C (T^u = 65 °C), and an ambient temperature of 20 °C (T^a = 20 °C) [19]. Each EWH has a storage capacity of 1500 kWh, and a power rating of 250 kW with 95% heating efficiency. To ensure the availability of hot water at any moment, the STOC of all EWHs is limited to a minimum of 30% ($SOTC^{min} = 0.3$). The microgrid is interfaced with the main grid through a 10 MVA transformer, and the minimum and maximum voltages at all buses are limited to 0.95 p.u. and 1.05 p.u., respectively.

The CL demand and hot water demand vary throughout the 24-hour period according to the half-hourly resolution profiles shown in Fig 6(a) and Fig 7, respectively. The one-minute resolution profile shown in Fig 6(b) is used to represent the variations of wind power generation. The values of CL demand, hot water demand and wind power used as predictions to evaluate the proposed control method were obtained from the profiles shown in Fig. 6 and Fig. 7. The predictions are obtained by shifting the profiles two control intervals to the left and calculating the mean value for each control interval. Thus, the predictions for the control interval $[t_i + \Delta^c, t_i + 2\Delta^c]$ are assumed to be equal to mean values obtained from the control interval $[t_i - \Delta^c, t_i]$ [24]. This approach is used for simplicity, since the development of a forecast method is not the focus of this work. The utilization of a more sophisticated forecast method is expected to improve the accuracy of the proposed control method. From the predicted values, 1000 scenarios of wind power are randomly generated for each control interval using the PDF (28). The scenario number is then reduced to 20 by applying the reduction technique described in the previous section. The predictions and scenarios of wind power for the period under analysis are shown in Fig 8. The imbalance prices for upward and downward deviations (κ_t^{up} and κ_t^{dn}) are assumed to be three times and half the day-ahead energy prices shown in fig 7 [36], respectively.

The performance of the proposed strategy to coordinate the operation of ESs for voltage regulation, congestion management, and cost minimization of the real-time energy deviations is evaluated by comparing the results of the following cases:

- Case 1: The microgrid is operated according to the proposed probabilistic rolling-optimization strategy.
- Case 2: The microgrid is operated according to the proposed

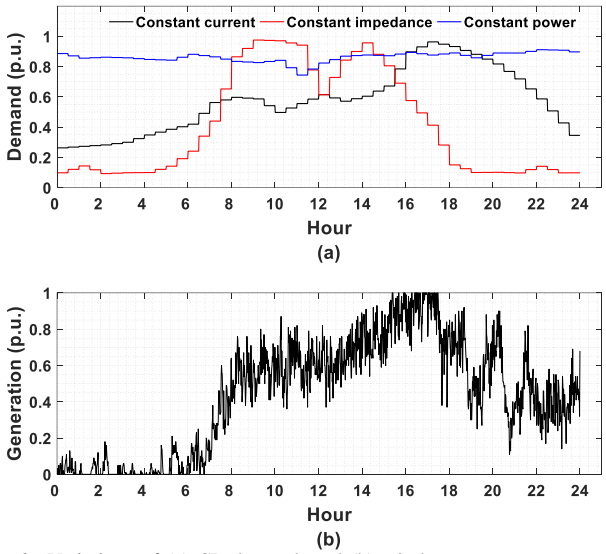

Fig. 6. Variations of (a) CL demand, and (b) wind power.

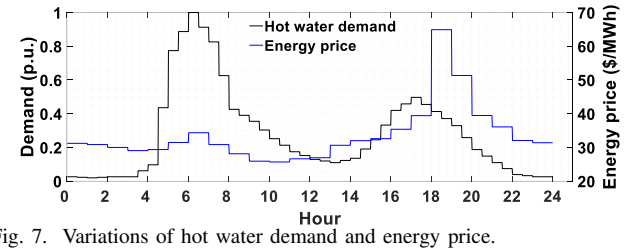

Fig. 7. Variations of hot water demand and energy price.

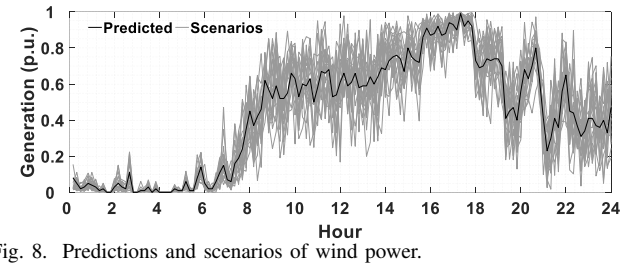

Fig. 8. Predictions and scenarios of wind power.

probabilistic rolling-optimization strategy but without considering ESs. This case simulates the EWHs controlled by the thermostat of their lower heating element. The EWHs are turned on and start consuming rated power when the SOTC reaches a lower threshold and are turned off when the water tank is full of hot water [7].

- Case 3: The microgrid is operated according to a deterministic formulation of the rolling-optimization strategy considering ESs. In this case, the optimization is performed for the predicted values of CL demand, hot water demand, and generation.

The above three cases were investigated for scenarios with 100% and 156% DG penetration level. Here, the DG penetration level is defined as the total DG installed capacity expressed as a percentage of the total peak load (CL plus NCL) in the microgrid. A DG penetration level of 156% corresponds to the maximum DG capacity that can be connected in the microgrid, and was obtained by applying a hosting capacity estimation method considering the operation of ESs [29]. A deterministic optimization model was formulated and solved to obtain the day-ahead scheduled power exchanges with the main grid ($P^s_{e,t}$) considering an hourly resolution [30], [31]. The objective function of the scheduling model is formulated to minimize the cost of the energy imports and maximize the revenue from the energy exports as follows:

$$\min \sum_{t\in\Omega_t} C^s_t P^s_{e,t}, \tag{32}$$

where, the energy prices C^s_t used in the scheduling model are shown in Fig 7. The variable $P^s_{e,t}$ takes positive values for energy imports and negative values for energy exports.

TABLE II
RESULTS WITH 100% DG PENETRATION LEVEL

	Case 1	Case 2
Imbalance Cost ($)	1416.60	1799.16
Upward deviation (MWh)	13.57	16.71
Downward deviation (MWh)	12.10	14.98

The performance of the optimal set points obtained for cases 1, 2 and 3 is assessed by running minute-by-minute power flow simulations with the data of CL demand, hot water demand and generation shown in Fig 6 and Fig 7. From these simulations, the microgrid operating state with one-minute resolution and the cost of energy deviations for the 24-hour period are obtained. The microgrid operating state is assessed with respect to bus voltage magnitudes, power flows in lines, adjustments to the scheduled energy exchanges, demand of EWHs, SOTC of EWHs and generation curtailment.

1) Reduction of the cost of energy deviations: A DG penetration level of 100% is considered to assess the performance of the proposed control strategy in reducing the cost of energy deviations in the microgrid. The total DG installed capacity is 8.8 MW distributed equally among the 4 indicated buses. The analysis is performed by comparing the results of cases 1 and 2. Under this DG penetration level, the microgrid does not experience violations to voltage and power flow limits, and generation curtailment is not necessary in both cases. Table II summarizes the results for the 24-hour period under analysis. Results show that the cost of energy deviations (imbalance cost) is reduced by 21% when ESs are used to regulate the energy consumption of EWHs. Upward and downward deviations in case 1 are lower than in case 2 because the EWH consumption is shifted to the time intervals with energy surplus, relieving the demand at the time intervals with energy deficit. The cost of energy deviations is reduced because of the difference between the prices for upward and downward deviations. That is, the price charged to the microgrid for upward deviations is higher than the price the microgrid is paid for downward deviations.

Figure 9 shows the hourly day-ahead scheduled power exchanges, and the real-time net load (critical load minus generation) and adjustments with one-minute resolution. In Fig 9(a), positive values indicate power imports and negative values power exports. In general, the magnitude and direction of the adjustments in real time depend on the magnitude of the day-ahead scheduled power exchanges and the net load in real time. Underestimating the scheduled power imports or overestimating the scheduled power exports implies the application of upward adjustments in real time to compensate for the energy deficit. Analogously, overestimating the sched-

uled power imports or underestimating the scheduled power exports implies the application of downward adjustments to compensate for the energy surplus. From Fig. 9(b) it can be seen that the use of ESs to control the EWHs consumption produces lower upward adjustments than the case without ESs most of the time.

The consumption profiles of the aggregated EWHs for cases 1 and 2 during the analyzed period are shown in Fig. 10. In case 2, without ESs, the EWHs start consuming at hour 7 and stop consuming at hour 21. These hours of consumption coincide with the period of highest wind power availability [see Fig 6(b)], which is an adequate operating rule when there is no possibility of dynamically controlling the EWHs. In case 1, the consumption pattern of the EWHs is optimally shaped to achieve the lowest cost of energy deviations. In this case, the ESs are operated to reduce the EWHs consumption at time intervals with energy deficit and supply the EWHs at time intervals with energy surplus. However, the consumption level of the EWHs is also conditioned by the SOTC of the EWHs and the energy imbalance price. For example, the EWHs consume rated power between hours 16–18 (which are hours with energy deficit) to store energy and use it later to supply the hot water demand at hours 19–21 when there are energy deficits and the imbalance price is higher.

The evolution of the SOTC of the EWHs operated with ESs (case 1) is shown in Fig. 11. STOCs below the adopted minimum (i.e., 0.3) are obtained because the ES voltage references are estimated based on predictions of wind power generation, critical load demand and hot water demand. However, it is observed that the proposed control strategy is effective in preventing the SOTCs from reaching values far below the minimum when the EWHs participate in demand side management and simultaneously supply the hot water demand. The highest SOTC is achieved at hour 6 because the EWHs store hot water to supply the peak demand at hours 7 and 8. A second highest SOTC is achieved at hour 18 when the EWHs store hot water to supply the demand at hours 19 and 20 when the power supplied to the EWHs is reduced to zero to compensate for the energy deficits, as observed from Fig. 9(b) and Fig. 10.

2) Voltage regulation and congestion management in the microgrid: The effectiveness of a probabilistic formulation of the control strategy to ensure adequate voltage and power flow levels in the microgrid was evaluated considering a 156% DG penetration level. The total DG installed capacity is 13.8 MW distributed as follows: 5.1 MW at bus 9, 2.4 MW at bus 10, 5.1 MW at bus 13 and 1.2 MW at bus 14. In this scenario, bus voltage and power flow limits violations are likely to occur if the operation of controllable resources is not adequately coordinated in real time. Fig. 12 shows the voltage profiles of bus 9 and the loading profiles of line segment 4–6 with one-minute resolution for cases 1, 2 and 3. Bus 9 and line segment 4–6 are selected for analysis because they are located in the feeder with the largest DG installed capacity. Bus 9 is the most distant from the point of common coupling in that feeder and line segment 4–6 concentrates the power flows coming from the DG at buses 9 and 10. Fig. 13 shows the maximum and minimum voltages reached at each bus during

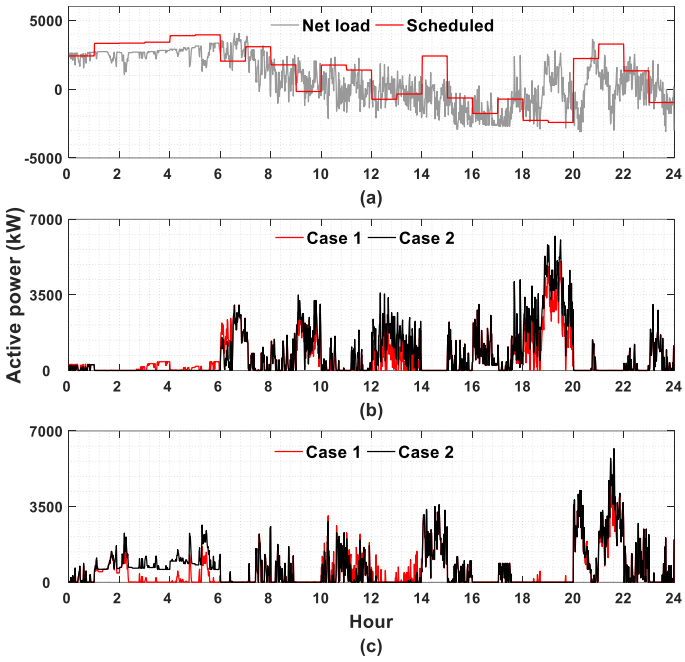

Fig. 9. (a) Net load and day-ahead scheduled power exchanges. (b) Upward adjustments. (c) Downward adjustments.

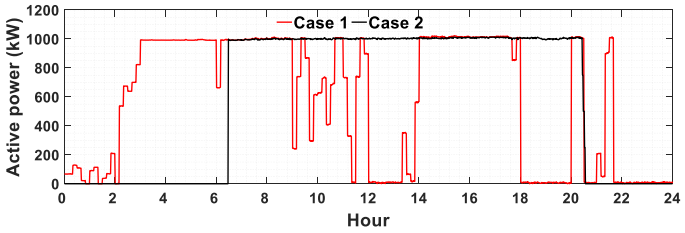

Fig. 10. Power demand of non-critical loads.

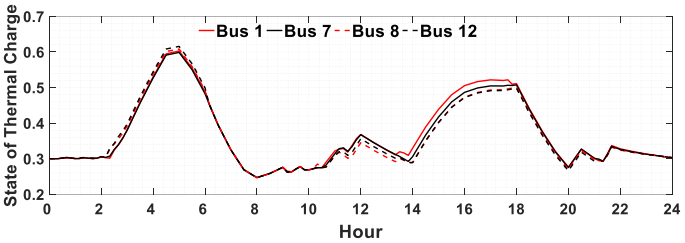

Fig. 11. State of thermal charge of EWHs for case 1.

the analyzed period. Note that, the profiles of cases 1 and 2 are similar and overlap most of the time. Both cases 1 and 2 are effective in limiting the duration and magnitude of voltage and line loading excursions outside the limits. This is possible because the optimal set points of controllable resources are estimated taking into account the possible realizations of wind power generation within each control interval through the probabilistic formulation. On the other hand, results of case 3 show that, with a deterministic approach, the voltage rise issues are not managed effectively and congestion exists for many minutes with line loading reaching 110 % of the maximum capacity.

Overvoltages and overloads can be avoided by applying generation curtailment and/or increasing the EWHs consumption because this reduces the reverse power flows. Fig. 14 shows the generation curtailment applied to the generator at bus 9

for the three cases. The consumption profiles of the EWH at bus 8 (which is the closest to the generator at bus 9) for the three cases are shown in Fig. 15. From these figures it can be seen that, in case 1 the EWH consumption is increased to the maximum at the time intervals with generation curtailment. Note that, the generation curtailment between hours 11 and 19 in cases 1 and 2 is the same and the curves overlap. This happens because during this period the EWH is turned on and drawing maximum power in case 2, which means that the EWH consumption in case 2 coincides with that of case 1 at the time intervals in which generation curtailment is applied. After hour 19, the generation curtailment in case 1 is lower than in case 2 because the flexibility provided by the ES allows the EWH to be controlled to draw maximum power while the EWH in case 2 is turned off. In this way, it is observed that the ESs can be used to control the EWHs consumption to reduce the need for generation curtailment.

Fig. 15 shows that the EWH consumption in case 3 is lower than in case 1 when the available wind power generation is near the maximum (i.e., hours 13-14 and 19-22). Moreover, in case 3 the generation curtailment is applied only when the available wind power generation is the maximum (see Fig. 14). As a result, the deterministic approach in case 3 fails to avoid overvoltages and overloads.

A summary of the results for the 24-hour period is shown in Table III. It is included the total number of minutes with bus voltage and power flow limits violations in the microgrid, the maximum reached line overload, and the maximum and minimum reached voltage magnitudes. The lowest cost of energy deviations is obtained in case 3, however, at the cost of increased congestion and voltage rise issues. This is because the optimality and feasibility of the microgrid operation is only ensured to the extent allowed by the information provided by the predicted values of demand and generation. Results of case 2 show that the probabilistic approach can manage congestion and voltage rise issues even without ESs by relying on the application of generation curtailment. However, the application of more generation curtailment and the impossibility of managing the EWHs consumption in case 2 translate into a 24.7% increase in the cost of energy deviations compared to case 3. In case 1, when ESs are available, the probabilistic approach can manage congestion and voltage rise issues with lower generation curtailment and cost of energy deviations than in case 2. In this case, the cost of energy deviations is 12.4% greater than in case 3, which represents half the increase in case 2. When compared with the deterministic case, the probabilistic formulation in cases 1 and 2 reduces the duration of overvoltages and line overloads by 50% and the magnitude of the maximum overvoltage and line overload by 75%.

3) Microgrid reactive power requirement: Since ESs exchange reactive power with the microgrid when regulating the voltage supplied to the EWHs, it is important to see how their operation impacts the reactive power requirements of the microgrid. Fig. 16 shows the total reactive power hours (varh) exchanged with the main grid during the 24-hour period for the cases with and without ESs, under the 100% and 156% DG penetration levels. In both cases, the microgrid behaves as an inductive source importing reactive power from the main grid

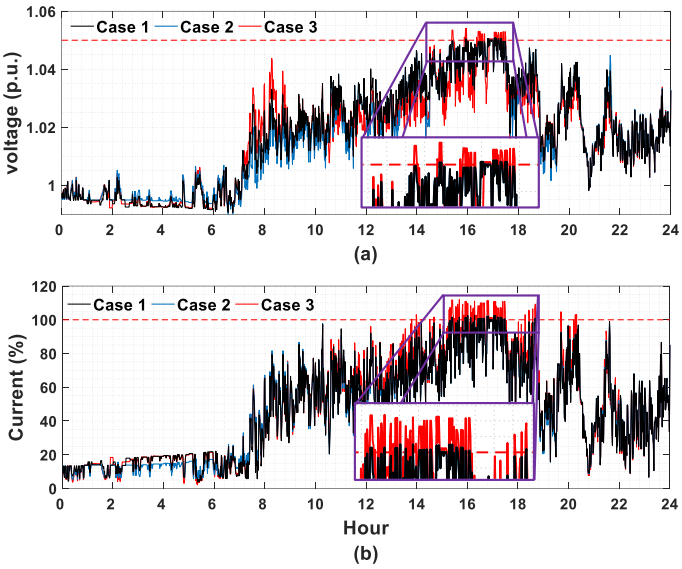

Fig. 12. (a) Voltages at bus 9 and (b) loading of line segment 4–6.

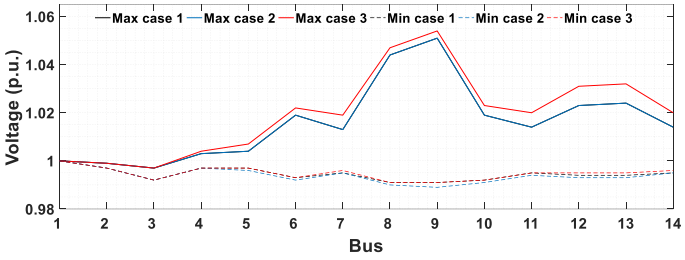

Fig. 13. Maximum and minimum voltages reached at each bus.

TABLE III
RESULTS WITH 156% DG PENETRATION LEVEL

	Case 1	Case 2	Case 3
Imbalance Cost ($)	2283.24	2533.73	2031.92
Upward deviation (MWh)	21.56	23.77	19.73
Downward deviation (MWh)	16.37	18.86	16.94
Generation curtailment (MWh)	2.14	2.37	0.14
Duration of line overloads (min)	41	41	85
Maximum line overload (%)	2.8	2.8	11.9
Duration of over/under voltages (min)	20	20	41
Maximum voltage (p.u.)	1.051	1.051	1.054
Minimum voltage (p.u.)	0.990	0.989	0.991

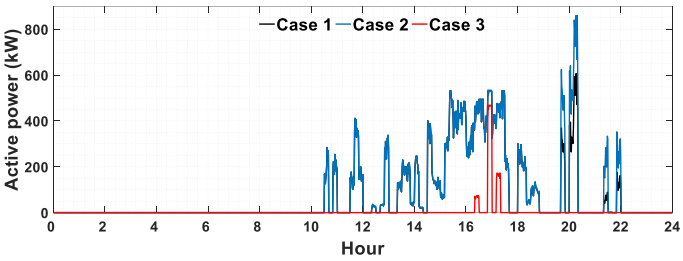

Fig. 14. Generation curtailment applied to the DG at bus 9.

at any time. The reactive power dispatch of the controllable resources (i.e., ES and DG) is determined by the optimization engine to produce the best results for the optimized microgrid operation. In case 1, ESs and DG work together to produce a lower microgrid reactive power requirement than case 2. The varh imports in case 1 with 100% and 156% DG penetration levels are, respectively, 26.8% and 19.8% lower than in case 2.

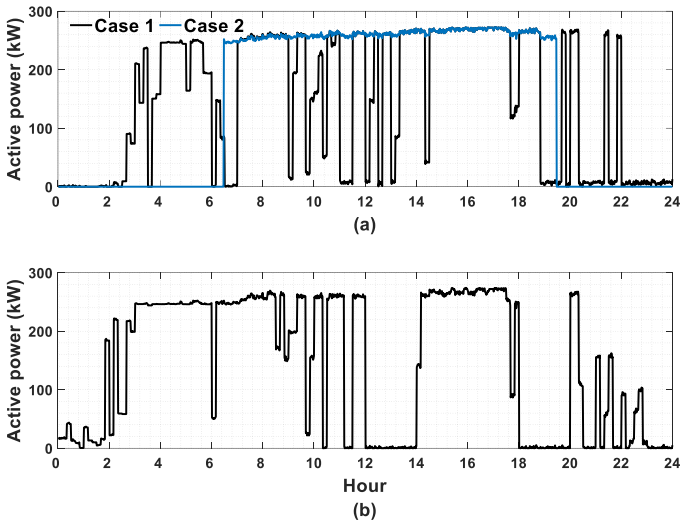

Fig. 15. Power demand of the EWH at bus 8 for (a) case 1 and 2, and (b) case 3.

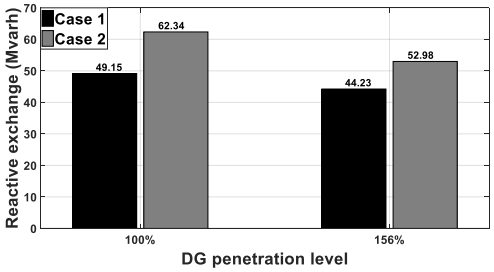

Fig. 16. Reactive power exchanges with the main grid.

It can also be seen that, in both cases, a 156% DG penetration level results in lower varh imports because the reactive power flows are reduced to free line capacity to transport the higher active power generation.

B. IEEE 33-bus system

The topology and line and load data of this system can be seen in [37]. This system has a nominal voltage of 12.66 kV and a total CL peak active power of 3.715 MW. The same specifications and assumptions adopted in the Guangdong system for the CLs, EWHs, DG, bus voltage limits, and energy prices are considered in this system. Smart loads are located at buses 11, 18, 24 and 31. It is considered a DG penetration level of 176% equivalent to 8.3 MW distributed as follow: 1.2 MW at bus 16, 2.8 MW at bus 25, and 4.3 MW at bus 33.

The performance of the proposed control strategy is evaluated by comparing the results of the three cases defined in section VI-A. A summary of the results for the 24-hour period is shown in Table IV. To reduce the duration and magnitude of the voltage and power flow limits violations, cases 1 and 2 increase the imbalance cost by 49.9% and 68.8%, respectively, compared to the results of case 3. It is also observed that the generation curtailment in case 1 is 36.7% lower than in case 2 due to the participation of ESs. Although the duration of the line overloads in case 3 is less than in cases 1 and 2, the maximum line overload reached in case 3 is 4 times greater. This system has longer lines than the Guangdog system and, therefore, it experiences more voltage issues including over and under voltages. Case 2

TABLE IV
RESULTS OBTAINED FOR THE 33-BUS TEST SYSTEM

	Case 1	Case 2	Case 3
Imbalance Cost ($)	1569.90	1767.45	1047.08
Upward deviation (MWh)	13.76	15.72	10.13
Downward deviation (MWh)	8.87	9.75	9.23
Generation curtailment (MWh)	3.50	5.53	0.00
Duration of line overloads (min)	42	39	7
Maximum line overload (%)	2.59	2.16	9.12
Duration of over/under voltages (min)	123	83	588
Maximum voltage (p.u.)	1.057	1.057	1.089
Minimum voltage (p.u.)	0.946	0.935	0.938

performs similarly to case 1 in reducing overvoltage issues due to the application of generation curtailment. However, case 1 performs better to solve undervoltage issues due the operation of ESs. In this case, the ESs reduce the EWHs consumption during the time intervals with high net load, thus reducing the magnitude of the undervoltages.

VII. CONCLUSION

In this paper, a rolling-optimization control strategy was proposed to coordinate the operation of multiple ESs to provide voltage regulation, congestion management and cost minimization of the real-time deviations from the scheduled energy exchanges with the grid in microgrids with wind-based DG. A probabilistic optimal power flow-based optimization engine was designed to find the optimal set points of ESs and generators every ten minutes based on predictions of demand and generation, and taking into account the variability and uncertainties of wind power generation.

Compared with a case in which EWHs were operated according to an on/off control scheme, the proposed approach reduced the cost of energy deviations by 21%. To achieve this, the optimization engine operated the ESs to shift the EWHs consumption to the hours with energy surplus and/or low upward imbalance price. When compared with a deterministic case, and considering a microgrid with high DG penetration, the probabilistic approach significantly reduced the magnitude and duration of bus voltage and line loading limits violations. Moreover, the participation of ESs helped to reduce the dependence on generation curtailment to manage microgrid constraints. The adoption of a realistic EWH model that considers electrical and thermal constraints allows to ensure users satisfaction when EWHs participate in demand side management. For future extension, it will be considered the integration of other DERs such as electric vehicles and dispatchable DG, and other types of NCLs with thermal cycle.

REFERENCES

[1] A. Keane, *et al.*, "State-of-the-art techniques and challenges ahead for distributed generation planning and optimization," *IEEE Trans. Power Syst.*, vol. 28, no. 2, pp. 1493-1502, 2013.
[2] J. S. Giraldo, *et al.*, "Microgrids energy management using robust convex programming," *IEEE Trans. Smart Grid*, vol. 10, no. 4, pp. 4520-4530, 2019.
[3] M. Nasr, *et al.*, "Assessing the effectiveness of weighted information gap decision theory integrated with energy management systems for isolated microgrids," *IEEE Trans. Ind. Informat.*, vol. 16, no. 8, pp. 5286-5299, 2020.
[4] L. I. Minchala-Avila, *et al.*, "Optimal energy management for stable operation of an islanded microgrid," *IEEE Trans. Ind. Informat.*, vol. 12, no. 4, pp. 1361-1370, 2016.

[5] M. Vahedipour-Dahraie, *et al.*, "Stochastic security and risk-constrained scheduling for an autonomous microgrid with demand response and renewable energy resources," *IET Renew. Power Gener.*, vol. 11, no. 14, pp. 1812-1821, 2017.

[6] E. Fuentes, L. Arce, and J. Salom, "A review of domestic hot water consumption profiles for application in systems and buildings energy performance analysis," *Renew. Sus. Energ. Rev.*, vol. 81, pp. 1530-1547, 2018.

[7] J. Kondoh, N. Lu, and D. J. Hammerstrom, "An evaluation of the water heater load potential for providing regulation service," *IEEE Trans. Power Syst.*, vol. 26, no. 3, pp. 1309-1316, 2011.

[8] S. Y. Hui, C. K. Lee, and F. F. Wu, "Electric springs a new smart grid technology," *IEEE Trans. Smart Grid*, vol. 3, no. 3, pp. 1552-1561, 2012.

[9] J. Soni, and S. K. Panda, "Electric spring for voltage and power stability and power factor correction," *IEEE Trans. Ind. Appl.*, vol. 53, no. 4, pp. 3871-3879, 2017.

[10] C. K. Lee, and S. Y. R. Hui, "Reduction of energy storage requirements in future smart grid using electric springs," *IEEE Trans. Smart Grid*, vol. 4, no. 3, pp. 1282-1288, 2013.

[11] X. Chen, *et al.*, "Mitigating voltage and frequency fluctuation in microgrids using electric springs," *IEEE Trans. Smart Grid*, vol. 6, no. 2, pp. 508-515, 2015.

[12] Z. Akhtar, B. Chaudhuri, and S. Y. R. Hui, "Primary frequency control contribution from smart loads using reactive compensation," *IEEE Trans. Smart Grid*, vol. 6, no. 5, pp. 2356-2365, 2015.

[13] X. Chen, Y. Hou, and S. Y. R. Hui, "Distributed control of multiple electric springs for voltage control in microgrid," *IEEE Trans. Smart Grid*, vol. 8, no. 3, pp. 1350-1359, 2017.

[14] T. Yang, *et al.*, "Use of integrated photovoltaic-electric spring system as a power balancer in power distribution networks," *IEEE Trans. Power Electron.*, vol. 34, no. 6, pp. 5312-5324, 2019.

[15] M. S. Javaid, *et al.*, "Design and implementation of electric spring for constant power applications," *Electr. Power Syst. Res.*, vol. 175, p. 105884, 2019.

[16] Y. Yang, *et al.*, "Reducing distribution power loss of islanded ac microgrids using distributed electric springs with predictive control," *IEEE Trans. Ind. Electron.*, vol. 67, no. 10, pp. 9001-9011, 2020.

[17] L. Liang, Y. Hou, and D. J. Hill, "An interconnected microgrids-based transactive energy system with multiple electric springs," *IEEE Trans. Smart Grid*, vol. 11, no. 1, pp. 184-193, 2020.

[18] L. Liang, *et al.*, "An optimal placement model for electric springs in distribution networks," *IEEE Trans. Smart Grid*, vol. 12, no. 1, pp. 491-501, 2021.

[19] T. Chen, *et al.*, "Distributed electric-spring-based smart thermal loads for overvoltage prevention in lv distributed network using dynamic consensus approach," *IEEE Trans. Sustain. Energy*, vol. 11, no. 4, pp. 2098-2108, 2020.

[20] J. Zhang, *et al.*, "Research on scheduling control strategy of large-scale air conditioners based on electric spring," *Int. J. Electr. Power Energy Syst.*, vol. 124, p. 106398, 2021.

[21] X. Luo, *et al.*, "Use of adaptive thermal storage system as smart load for voltage control and demand response," *IEEE Trans. Smart Grid*, vol. 8, no. 3, pp. 1231-1241, 2017.

[22] L. Liang, Y. Hou, and D. J. Hill, "Enhancing flexibility of an islanded microgrid with electric springs," *IEEE Trans. Smart Grid*, vol. 10, no. 1, pp. 899-909, 2019.

[23] E. Planas, *et al.*, "General aspects, hierarchical controls and droop methods in microgrids: A review," *Renew. Sustain. Energy Rev.*, vol. 17, pp. 147-159, 2013.

[24] H. Bludszuweit, J. A. Dominguez-Navarro, and A. Llombart, "Statistical analysis of wind power forecast error," *IEEE Trans. Power Syst*, vol. 23, no. 3, pp. 983-991, 2008.

[25] S. Bonfinger, A. Luig, and H. G. Bayer, "Qualification of wind power forecast," in *2002 Global Windpower Conference*, 2002, pp. 1-5.

[26] D. A. Quijano, and A. Padilha-Feltrin, "Optimal integration of distributed generation and conservation voltage reduction in active distribution networks," *Int. J. Electr. Power Energy Syst.*, vol. 113, pp. 197-207, 2019.

[27] A. G. Vlachos, and P. N. Biskas, "Demand response in a real-time balancing market clearing with pay-as-bid pricing," *IEEE Trans. Smart Grid*, vol. 4, no. 4, pp. 1966-1975, 2013.

[28] J. Fernandez-Seara, F. J. Uhia, and J. Sieres "Experimental analysis of a domestic electric hot water storage tank. Part II: dynamic mode of operation," *Appl. Therm. Eng.*, vol. 27, no. 1, pp. 137-144, 2007.

[29] D. A. Quijano, *et al.*, "Stochastic assessment of distributed generation hosting capacity and energy efficiency in active distribution networks," *IET Gener. Trans. Dist.*, vol. 11, no. 18, pp. 4617-4625, 2017.

[30] S. M. Nosratabadi, R.-A. Hooshmand, and E. Gholipour, "A comprehensive review on microgrid and virtual power plant concepts employed for distributed energy resources scheduling in power systems," *Renew. Sust. Energ. Rev.*, vol. 67, pp. 341-363, 2017.

[31] S. Liu, *et al.*, "Effects of correlated photovoltaic power and load uncertainties on grid-connected microgrid day-ahead scheduling," *IET Gener. Trans. Dist.*, vol. 11, no. 14, pp. 3620-3627, 2017.

[32] H. G. Yeh, D. F. Gayme, and S. H. Low, "Adaptive var control for distribution circuits with photovoltaic generators," *IEEE Trans. Power Syst*, vol. 27, no. 3, pp. 1656-1663, 2012.

[33] H. Heitsch, and W. Römisch, "Scenario reduction algorithms in stochastic programming," *Comput. Optim. Appl.*, vol. 24, no. 2, pp. 187-206, 2003.

[34] Y. Dvorkin, *et al.*, "Comparison of scenario reduction techniques for the stochastic unit commitment," in *Proc. 2014 IEEE Power and Energy Society General Meeting*, National Harbor, MD, USA, 2014, pp. 1-5.

[35] W. Shi, *et al.*, "Distributed optimal energy management in microgrids," *IEEE Trans. Smart Grid*, vol. 6, no. 3, pp. 1137-1146, 2015.

[36] R. A. C. Veen, A. Abbasy, and R. Hakvoort, "A comparison of imbalance settlement designs and results of germany and the netherlands," in *Proc. Working Paper Young Energy Eng. Economists Seminar (YEEES)*, 2010, pp. 1-24.

[37] M. Baran, and F. Wu, "Network reconfiguration in distribution systems for loss reduction and load balancing," *IEEE Trans. Power Del.*, vol. 4, no. 2, pp. 1401-1407, 1989.